



HHS Public Access

Author manuscript

Bioorg Med Chem Lett. Author manuscript; available in PMC 2021 August 15.

Published in final edited form as:

Bioorg Med Chem Lett. 2020 August 15; 30(16): 127292. doi:10.1016/j.bmcl.2020.127292.

Targeting the TS dimer interface in bifunctional *Cryptosporidium hominis* TS-DHFR from parasitic protozoa: virtual screening identifies novel TS allosteric inhibitors

Victor G. Ruiz^a, Daniel J. Czyzyk^a, Vidya P. Kumar^{a,b,c}, William L. Jorgensen^b, Karen S. Anderson^{a,c,*}

^aDepartment of Pharmacology, Yale University School of Medicine, 333 Cedar Street, New Haven, CT 06520, USA

^bDepartment of Chemistry, Yale University, 225 Prospect Street, PO Box 208107, New Haven, CT 06520-8107, USA

^cDepartment of Molecular Biophysics and Biochemistry, Yale University School of Medicine, 333 Cedar Street, New Haven, CT 06520, USA

Abstract

Effective therapies are lacking to treat gastrointestinal infections caused by the genus *Cryptosporidium*, which can be fatal in the immunocompromised. One target of interest is *Cryptosporidium hominis* (*C. hominis*) thymidylate synthase-dihydrofolate reductase (*Ch*TS-DHFR), a bifunctional enzyme necessary for DNA biosynthesis. Targeting the TS-TS dimer interface is a novel strategy previously used to identify inhibitors against the related bifunctional enzyme in *Toxoplasma gondii*. In the present study, we target the *Ch*TS dimer interface through homology modeling and high-throughput virtual screening to identifying allosteric, *Ch*TS-specific inhibitors. Our work led to the discovery of methylenedioxyphenyl-aminophenoxypropanol analogues which inhibit *Ch*TS activity in a manner that is both dose-dependent and influenced by the conformation of the enzyme. Preliminary results presented here include an analysis of structure activity relationships and a *Ch*TS-apo crystal structure of *Ch*TS-DHFR supporting the continued development of inhibitors that stabilize a novel pocket formed in the open conformation of *Ch*TSTS.

Keywords

Cryptosporidium hominis; Cryptosporidiosis; Thymidylate synthase; TS-DHFR; allosteric inhibitor; TS/TS interface; Virtual Screen; GLIDE; X-ray Crystallography

Cryptosporidium hominis (*C. hominis*) is an apicomplexan parasite found on every continent except Antarctica which causes moderate-to-severe gastrointestinal illness

*Corresponding authors. Tel.: +1 203 785 4526; fax: +1 203 785 7670 (K.S.A.). karen.anderson@yale.edu (K.S. Anderson).

Publisher's Disclaimer: This is a PDF file of an unedited manuscript that has been accepted for publication. As a service to our customers we are providing this early version of the manuscript. The manuscript will undergo copyediting, typesetting, and review of the resulting proof before it is published in its final form. Please note that during the production process errors may be discovered which could affect the content, and all legal disclaimers that apply to the journal pertain.

(cryptosporidiosis) in humans. The 2012 Global Enteric Multicenter Study in resource-poor[1] countries identified cryptosporidiosis as the second-leading cause of diarrheal disease and deaths in children <2 years old.[2–5] Additionally, outbreaks of cryptosporidiosis have occurred in industrialized countries, and is responsible for 58% of recreational water-associated disease attributed to infectious organisms in the United States from 2000–2014.[6–8] *C. parvum*, which is genetically similar to *C. hominis*, is capable of surviving without a host for many months and at a wide range of temperatures.[9–12] Infection occurs when an individual ingests the parasite in contaminated food or water. In immunocompetent individuals, it is often a transient, self-limiting illness. However, in immunocompromised individuals, children, and the elderly, infections from *C. hominis* can cause serious complications, including muscle wasting and death, due to cellular ablation and malabsorption in the gastrointestinal tract.[13–16] Currently, nitazoxanide is the only FDA-approved drug for the treatment of cryptosporidiosis, but due to its limited efficacy there is a pressing need for improved therapies and therapeutic targets.[2, 17, 18]

One protein which has been extensively studied and validated as a therapeutic target in *C. hominis* is thymidylate synthase-dihydrofolate reductase (*Ch*TS-DHFR), a bifunctional enzyme in parasitic protozoa that is necessary for DNA biosynthesis and survival.[19, 20] TS catalyzes the transfer of a methylene group from 5,10-methylene tetrahydrofolate ($\text{CH}_2\text{H}_4\text{F}$) to deoxyuridine monophosphate (dUMP) to produce deoxythymidine monophosphate (dTMP) necessary for DNA replication with dihydrofolate (H_2F) as a byproduct. DHFR utilizes NADPH in order to reduce H_2F to tetrahydrofolate (H_4F). While most drug discovery efforts against TS-DHFR from protozoan parasites have focused on inhibiting catalytic activity of DHFR or TS,[21–23] targeting non-active site regions in the bifunctional enzyme of parasites has become increasingly recognized as a desirable strategy for improving drug selectivity and overcoming active site resistance mutations.[7, 24–26]

As with human TS, proper orientation of the TS domain in *Ch*TS-DHFR and arrangement of active site residues is required for catalysis to occur.[27–31] Specifically, catalysis requires that TS dimerize such that conserved arginine residues from one monomer transverse the dimer interface and form contacts with incoming dUMP in the adjacent monomer.[31, 32] Since TS exists in equilibrium between its active and inactive conformations,[30, 33, 34] dUMP binding helps stabilize TS in its active conformation, while the apo-structure without dUMP favors the inactive conformation.[30, 34]

Previous studies have shown that peptides can be designed to target the dimer interface of human TS, stabilize the inactive conformation, and, therefore, disrupt catalytic activity.[35, 36] Two such peptides were crystallized with human TS in its inactive conformation, revealing a new pocket formed by an opening at the base of the TS/TS interface (PDB IDs: 3N5E, 4FGT). The TS/TS interface pocket is generally absent in both dUMP-apo and dUMP-liganded human TS structures;[35, 37] therefore, formation of the new pocket in 3N5E and 4FGT appears to be dependent on peptide binding. The two crystallized peptides form a disulfide bond with Cys-180 in the new pocket, suggesting that targeting specific residues at the TS/TS interface may be a promising strategy for the discovery of novel TS allosteric inhibitors.

The case for inhibiting TS activity allosterically is further supported by a peptidomimetic study from our group focused on a related bifunctional protozoal enzyme from *Toxoplasma gondii*.^[24] This effort revealed that short peptides can be designed to non-competitively inhibit *T. gondii* TS activity. Moreover, since the sequence for the parasitic enzymes is distinct in the TS/TS interface region compared with the human TS enzyme, inhibition was selective for the *T. gondii* TS activity.^[24] This early work provided the first evidence that the TS/TS interface can be targeted in bifunctional enzymes, not just monofunctional ones like human TS. A subsequent virtual screen campaign by our group resulted in the discovery of small molecules with non-competitive inhibition against TS activity in *T. gondii* TS.^[38] In the virtual screen study, homology modeling was used to generate a model of *T. gondii* TS with a TS/TS interface pocket like the one found in the peptide-bound human TS structure.^[38]

In principle, a similar strategy can be used to search for allosteric inhibitors of TS from *C. hominis*. In the present study, we set out to target the *ChTS* dimer interface by homology modeling and high-throughput virtual screening with the goal of identifying allosteric, *ChTS*-specific inhibitors. Our work led to the discovery of analogues originating from the Maybridge Diversity Library which inhibit *ChTS* activity in a manner that is both dose-dependent and influenced by the conformation of the enzyme. Our experimental approach, as well as a discussion of the results and implications from our work, are described below.

As illustrated in Figure 1, we used the Structure Prediction Wizard from Schrödinger to generate a homology model of *ChTS* containing the TS/TS interface pocket by matching the amino acid sequence of *ChTS* to the peptide-bound human TS structure (PDB ID: 3N5E). As with the human TS structure, the interface region at the base of the dimer complex in the *C. hominis* homology model was now more open, revealing a novel pocket not previously observed in *ChTS* crystallographically. The SiteMap tool from Schrödinger was used to evaluate the ligandability of the new pocket and produced a SiteScore > 1.0, suggesting high similarity in size, volume, and hydrophilic character with known ligand-binding pockets. Notably, the pocket consists of a buried hydrophobic cavity at its center and extends to a solvent-exposed surface with hydrophilic residue contributions from both monomers (right of Figure 1).

An alignment of backbone atoms between the peptide-bound human TS and *C. hominis* homology model structures reveals good agreement between the two (0.165 Å RMSD), which is expected given the >50% sequence identity (Supplemental Figure 1). The major difference is that residues Phe-142, Gly-143, and Cys-180 in human TS are residues Tyr-349, Asn-350, and Thr-387, respectively, in the *C. hominis* enzyme (Figure 2). We took advantage of these differences by targeting *ChTS*-specific residues at the TS/TS interface using high-throughput virtual screening. Docking was performed in successive standard precision (SP) and extra precision (XP) modes in Glide using the 20,000 compound Maybridge Diversity library. This library was selected for having a range of chemotypes with drug-like properties that are available commercially. From 26 compounds matching our filter criteria, ten were obtained from the Yale Center for Molecular Discovery for screening and additional compounds were obtained from commercial sources where available.

Our assay consisted of monitoring *ChTS*-catalyzed turnover of radiolabeled $\text{CH}_2\text{H}_4\text{F}$ to H_2F by HPLC and radioactivity flow detection in the presence of compound. As a first step, *ChTS*-DHFR was incubated with compound for 30 minutes before adding dUMP and $\text{CH}_2\text{H}_4\text{F}$ to start the reaction. Since dUMP binding is known to stabilize the active conformation of *ChTS*, incubating the compound with enzyme for 30 minutes before adding dUMP would make the inactive conformation of the enzyme more accessible to binding. Results from the inhibition assay are shown in Figure 3A, and included in Table 1 along with Glide XP scores. Four compounds, **2**, **6**, **7**, and **10**, were determined to significantly inhibit *ChTS* activity in the presence of 500 μM compound [(76 \pm 9)%, (83 \pm 1)%, (46.0 \pm 0.8)%, and (55 \pm 1)%, respectively]. Notably, the three compounds with the highest percent inhibition, **2**, **6**, and **10**, have the same methylenedioxyphenyl-aminophenoxypropanol chemotype (Figure 3b).

We examined the binding modes of **2**, **6**, and **10** to identify possible structure activity relationships. In all three, the common chemotype is solvent-exposed and directed away from the center of the pocket towards the exposed surface of one of the monomers (Supplemental Figure 2). The major differences in binding are with respect to functional group substitutions on the phenyl ring of the anisole moiety, which is directed towards the interior of the pocket. For example, **2** contains a thiadiazole ring at the C-4 position which enables it to penetrate deeper into the buried hydrophobic cavity compared to **6** and **10**, which do not have a ring substitution on the anisole ring (Supplemental Figure 2). However, compound **6**, which demonstrates the highest level of inhibition among the three, has chloro and bromo groups in the buried anisole ring, allowing it to penetrate the cavity with a much larger volume. The higher entropic contribution to the binding free energy resulting from this difference, as well as greater enthalpic contributions from halogen bonding to interface pocket residues, may help explain why **6** exhibits better inhibition. The predicted binding mode for **6** is shown in Figure 4.

To further evaluate the chemical space of *ChTS*-TS interface inhibitors, we performed a structure activity relationship (SAR) study using commercially-available compounds containing the same methylenedioxyphenyl-aminophenoxypropanol chemotype as **2**, **6**, and **10** from our virtual screen. As illustrated in Table 2, several of the derivative compounds displayed significant inhibitory activity at 500 μM . Compound **14**, which is similar to compound **2** (Figure 5), has a hydrophobic benzyl substituent at the C-4 position of the anisole moiety and displayed the greatest inhibitory activity at (87 \pm 1)%. Compound **18** is most similar to compound **6** (Figure 5) and contains a C-4 chloride substituent in combination with another halogen substituent in the anisole moiety for an inhibition activity of (83 \pm 1) %. Also noteworthy are the similarities between compounds **10** and **17** (Table 2), which contain hydrophobic methyl substituents in the anisole moiety and displayed ~50 % inhibition. Among the least inhibitory were compounds which contained an o-methoxy group at the C-2 position (Table 2). Interestingly, removal of the o-methyl group in **6** to produce **19** (Table 2) resulted in a ~3-fold increase in inhibitory activity, suggesting that polar atoms in the anisole ring are detrimental to protein-ligand binding. Finally, converting the anisole moiety to either a phenylthiol or thiophenylthiol moiety, as in **11** and **12** (Table 2), resulted in moderate levels of inhibitory activity, (34 \pm 4) % and (43 \pm 11) %, respectively.

respectively, thus providing a useful reference point for evaluating the effect of hydrophobicity of anisole substituents on inhibition. Taken together, these results suggest that large, hydrophobic substituents on the anisole ring are important for ligand interactions with hydrophobic residues in the buried cavity of the *Ch*TS-TS interface. Based on their potency in the *Ch*TS inhibition assay, compounds **2**, **6**, **14**, and **18** were selected for further characterization.

Keeping in mind that *Ch*TS-DHFR is a bifunctional enzyme, we next tested whether the compounds might also be inhibiting *Ch*DHFR activity to assess whether the inhibition is selective for *Ch*TS activity and also to rule out nonspecific effects that may be due to compound aggregation. The evaluation of DHFR activity was accomplished using a previously-described radiometric assay to monitor the conversion of radiolabeled H₂F to H₄F by HPLC and determine the % *Ch*DHFR inhibition.[26, 39]

We found that **2** had negligible inhibition on *Ch*DHFR activity ($6 \pm 10\%$), while **6** and **14** had a small inhibitory effect, ($19 \pm 5\%$) and ($26 \pm 6\%$), respectively (Figure 6). Compound **18** displayed the highest inhibition of *Ch*DHFR activity at ($60 \pm 4\%$) (Figure 6). This data suggests **2**, **6**, and **14** are specific for *Ch*TS. Furthermore, this data suggests that **2**, **6**, and **14** inhibit *Ch*TS activity through a mechanism independent from colloidal aggregation, while the inhibition of *Ch*TS by **18** may result from some amount of compound aggregation. Compound **6** displayed the best balance of potency and specificity for *Ch*TS and was therefore selected for further characterization.

Whereas our initial screen consisted of pre-incubating the enzyme with compound before adding dUMP, we next tested whether changing the order of addition of dUMP to stabilize the active conformation of *Ch*TS might influence the pattern of inhibition initially observed. In addition, for both the dUMP-apo and dUMP-liganded conditions, we tested multiple concentrations of compound to test whether the inhibition observed was dose-dependent. As a first step, *Ch*TS-DHFR was mixed with dUMP and allowed to incubate for 5 minutes before adding inhibitor and later CH₂H₄F to start the reaction. The prediction is that compound **6** would have better inhibition against the dUMP-apo form of the enzyme representing the inactive conformation.

From the order-of-addition and dose-response experiments, it appears that **6** displays a preference for the inactive conformation of the enzyme (Figure 7). This was evident by the increase in IC₅₀ from $172 \pm 11 \mu\text{M}$ in the dUMP-apo condition to an IC₅₀ of $304 \pm 16 \mu\text{M}$ in the dUMP-liganded condition. These results suggest that compound **6** preferentially binds to the inactive conformation of *Ch*TS and that inhibition from both compounds is dose-dependent. Finally, although our virtual screen protocol was designed to target residues that are unique to *Ch*TS, it is possible that compound **6** still retains some ability to bind the human enzyme. We determined the specificity of **6** for *Ch*TS versus human TS. The compound was incubated with the TS enzyme in the absence of dUMP to evaluate its potential inhibitory effects. While **6** inhibited the activity of human TS by ~50% at 500 uM, it displayed about a two-fold selectivity for *Ch*TS (Figure 8).

Finally, to gain a better understanding of the important interactions between our inhibitors and the *ChTS*-TS interface pocket, we performed crystallization experiments. While we were unsuccessful in obtaining a co-crystal structure with any of the virtual screen inhibitors, we very recently solved a structure of *ChTS*-DHFR (PDB ID 6WEP) in which dUMP and folate are not bound to the *ChTS* active site, similar to human TS structures 3N5E and 4FGT. The 6WEP structure contains two protein molecules within the asymmetric subunit and crystallized as a P2₁2₁2₁ space group with a resolution of 2.79 Å. Since this is the first time a TS-apo structure has been solved for TS-DHFR from *C. hominis*, we explored the possibility that the conformation of the interface region may be more open and therefore better accommodate *ChTS* interface inhibitors.

We compared the *ChTS*-apo structure with a *ChTS*-DHFR crystal structure of similar resolution containing dUMP and a folate analogue bound to the TS active site (PDB ID 6PF7; Supplemental Figure 3A). Overall, both structures are very similar, though the *ChTS*-TS interface region of the *ChTS*-apo structure appears to be in a slightly more open conformation relative to the structure with dUMP bound. However, the overlay in Supplemental Figure 3B revealed that the conformation observed in the *ChTS*-apo structure is significantly less open than the *ChTS* homology model we generated in Figure 1. This difference is understandable considering that the homology model in Figure 1 was prepared using a crystal structure of human TS in which the *ChTS*-TS interface region was “locked” in an open conformation by covalent linkage with a peptide inhibitor. Taken together, these results suggest that incorporating a sulfhydryl group or other cysteine reactive moiety to the anisole ring of our methylenedioxyphenyl-aminophenoxypropanol derivatives within the size constraints of the pocket may be a promising strategy to stabilize the *ChTS*-TS interface in an open conformation and allow for co-crystallization.

In summary, we have discovered novel inhibitors of *C. hominis* TS activity from the Maybridge Diversity Library using a combined homology modeling and virtual screen approach targeting the *ChTS*/TS dimer interface. This is the first time this approach has been used to target a non-active site pocket of the TS domain from *ChTS*-DHFR. Three commercially-available analogues from our screen, **2**, **6**, and **14** demonstrated greater specific for *ChTS* over *ChDHFR*. Because *ChDHFR* activity was not significantly affected, the inhibition observed for **2**, **6**, and **14** is unlikely to be due to compound aggregation. Compound **6** from this group was further characterized and found to preferentially bind to the dUMP-apo/inactive conformation of *ChTS*, with a ~2-fold preference over the dUMP-liganded form. In studies previously conducted by our lab a 2.6-to-2.7-fold preference for the inactive conformation was observed with small-molecule inhibitors of the TS/TS interface in bifunctional *TgTS*-DHFR.[38] Similarly, crystal structures of human TS with a peptide bound at the TS/TS interface (PDB IDs 3N5E and 4FGT) do not have dUMP bound and TS is in the inactive conformation.[35, 36] Since a preference for the dUMP-apo/inactive conformation is characteristic of TS/TS interface-mediated inhibition in *TgTS*, human TS, and *Lactobacillus casei* TS,[40] our results suggest that **6** inhibits *ChTS* by binding to the TS/TS interface.

Interestingly, the best inhibitors from our study share the same methylenedioxyphenyl-aminophenoxypropanol chemotype. In the absence of co-crystallographic information, it is

not fully clear what role this chemotype plays in binding the TS/TS interface pocket in *C. hominis*. However, the fact that this chemotype was successfully enriched in 3 out of 10 compounds resulting from our screen and further validated with 11 additional compounds in our SAR analysis suggests that it plays a role in *ChTS* inhibition and is worth pursuing with further optimization. Co-crystallization studies are currently underway, with preliminary results supporting the development of covalent inhibitors that bind to and stabilize the pocket formed in the open conformation of the *ChTS*-TS interface.

Supplementary Material

Refer to Web version on PubMed Central for supplementary material.

Acknowledgements

This work is supported by NIH Grant (AI083146) to K.S.A., NIH Grant (GM32136) to W.L.J. This work is based upon research conducted at the Northeastern Collaborative Access Team beamlines, which are funded by the National Institute of General Medical Sciences (NIGMS) from the NIH [P41 GM103403]. Crystals screening was conducted with supports in the Yale Macromolecular X-ray Core Facility [1S10OD018007-01]. This research used resources of the Advanced Photon Source, a U.S. Department of Energy (DOE) Office of Science User Facility operated for the DOE Office of Science by Argonne National Laboratory under Contract No. DEAC02-06CH11357. This research used FMX beamline of the National Synchrotron Light Source II, a U.S. Department of Energy (DOE) Office of Science User Facility operated for the DOE Office of Science by Brookhaven National Laboratory under Contract No. DE-SC0012704. The Life Science Biomedical Technology Research resource is primarily supported by the NIH, NIGMS through a Biomedical Technology Research Resource P41 grant (P41 GM111244), and by the DOE Office of Biological and Environmental Research (KP1605010). We would like to thank James B. Herrington at the Yale Center for Molecular Discovery for his generosity in providing us with screening compounds.

References

- [1]. Behera B, Mirdha BR, Makharia GK, Bhatnagar S, Dattagupta S, Samantaray JC, Parasites in patients with malabsorption syndrome: a clinical study in children and adults, *Dig Dis Sci*, 53 (2008) 672–679. [PubMed: 17763958]
- [2]. Checkley W, White AC Jr., Jaganath D, Arrowood MJ, Chalmers RM, Chen XM, Fayer R, Griffiths JK, Guerrant RL, Hedstrom L, Huston CD, Kotloff KL, Kang G, Mead JR, Miller M, Petri WA Jr., Priest JW, Roos DS, Striepen B, Thompson RC, Ward HD, Van Voorhis WA, Xiao L, Zhu G, Houpt ER, A review of the global burden, novel diagnostics, therapeutics, and vaccine targets for cryptosporidium, *Lancet Infect Dis*, 15 (2015) 85–94. [PubMed: 25278220]
- [3]. Kotloff KL, Nataro JP, Blackwelder WC, Nasrin D, Farag TH, Panchalingam S, Wu Y, Sow SO, Sur D, Breiman RF, Faruque AS, Zaidi AK, Saha D, Alonso PL, Tamboura B, Sanogo D, Onwuchekwa U, Manna B, Ramamurthy T, Kanungo S, Ochieng JB, Omore R, Oundo JO, Hossain A, Das SK, Ahmed S, Qureshi S, Quadri F, Adegbola RA, Antonio M, Hossain MJ, Akinsola A, Mandomando I, Nhampossa T, Acacio S, Biswas K, O'Reilly CE, Mintz ED, Berkeley LY, Muhsen K, Sommerfelt H, Robins-Browne RM, Levine MM, Burden and aetiology of diarrhoeal disease in infants and young children in developing countries (the Global Enteric Multicenter Study, GEMS): a prospective, case-control study, *Lancet*, 382 (2013) 209–222. [PubMed: 23680352]
- [4]. Miller CN, Panagos CG, Mosedale WRT, Kvac M, Howard MJ, Tsaousis AD, NMR metabolomics reveals effects of *Cryptosporidium* infections on host cell metabolome, *Gut Pathog*, 11 (2019) 13. [PubMed: 30984292]
- [5]. Dayao DA, Sheoran A, Carvalho A, Xu H, Beamer G, Widmer G, Tzipori S, An immunocompetent rat model of infection with *Cryptosporidium hominis* and *Cryptosporidium parvum*, *Int J Parasitol*, (2019).
- [6]. Kissinger JC, Evolution of *Cryptosporidium*, *Nat Microbiol*, 4 (2019) 730–731. [PubMed: 31015741]

- [7]. Martucci WE, Udier-Blagovic M, Atreya C, Babatunde O, Vargo MA, Jorgensen WL, Anderson KS, Novel non-active site inhibitor of *Cryptosporidium hominis* TS-DHFR identified by a virtual screen, *Bioorg Med Chem Lett*, 19 (2009) 418–423. [PubMed: 19059777]
- [8]. McAteer J, Jernigan S, Mao C, Gonzalez MD, Watson RJ, Liverman R, Tobin DAM, Dishman MH, Shane A, Yildirim I, Cryptosporidiosis among solid organ transplant recipient attendees at a summer camp, *Pediatr Transplant*, (2019) e13649. [PubMed: 31885132]
- [9]. Reinoso R, Becares E, Smith HV, Effect of various environmental factors on the viability of *Cryptosporidium parvum* oocysts, *J Appl Microbiol*, 104 (2008) 980–986. [PubMed: 17973913]
- [10]. Fayer R, Trout JM, Jenkins MC, Infectivity of *Cryptosporidium parvum* oocysts stored in water at environmental temperatures, *J Parasitol*, 84 (1998) 1165–1169. [PubMed: 9920307]
- [11]. Peng X, Murphy T, Holden NM, Evaluation of the effect of temperature on the die-off rate for *Cryptosporidium parvum* oocysts in water, soils, and feces, *Appl Environ Microbiol*, 74 (2008) 7101–7107. [PubMed: 18849452]
- [12]. Duhain GL, Minnaar A, Buys EM, Effect of chlorine, blanching, freezing, and microwave heating on *Cryptosporidium parvum* viability inoculated on green peppers, *J Food Prot*, 75 (2012) 936–941. [PubMed: 22564944]
- [13]. Bouzid M, Hunter PR, Chalmers RM, Tyler KM, *Cryptosporidium* pathogenicity and virulence, *Clin Microbiol Rev*, 26 (2013) 115–134. [PubMed: 23297262]
- [14]. Goodgame RW, Kimball K, Ou CN, White AC Jr., Genta RM, Lifschitz CH, Chappell CL, Intestinal function and injury in acquired immunodeficiency syndrome-related cryptosporidiosis, *Gastroenterology*, 108 (1995) 1075–1082. [PubMed: 7698574]
- [15]. Ribeiro Machado F, Gonzaga Vaz Coelho L, Chausson Y, Greco DB, Fat malabsorption assessed by ¹⁴C-triolein breath test in HIV-positive patients in different stages of infection: is it an early event?, *J Clin Gastroenterol*, 30 (2000) 403–408. [PubMed: 10875469]
- [16]. Sciarretta G, Bonazzi L, Monti M, Furno A, Mazzoni M, Mazzetti M, Gritti F, Malaguti P, Bile acid malabsorption in AIDS-associated chronic diarrhea: a prospective 1-year study, *Am J Gastroenterol*, 89 (1994) 379–381. [PubMed: 8122649]
- [17]. Borad A, Ward H, Human immune responses in cryptosporidiosis, *Future Microbiol*, 5 (2010) 507–519. [PubMed: 20210556]
- [18]. Grayson ML, Kucers' the use of antibiotics: a clinical review of antibacterial, antifungal, antiparasitic and antiviral drugs, Seventh edition ed., CRC Press, Boca Raton, 2017.
- [19]. O'Neil RH, Lilien RH, Donald BR, Stroud RM, Anderson AC, Phylogenetic classification of protozoa based on the structure of the linker domain in the bifunctional enzyme, dihydrofolate reductase-thymidylate synthase, *J Biol Chem*, 278 (2003) 52980–52987. [PubMed: 14555647]
- [20]. Mukerjee A, Iyidogan P, Castellanos-Gonzalez A, Cisneros JA, Czyzyk D, Ranjan AP, Jorgensen WL, White AC Jr., Vishwanatha JK, Anderson KS, A nanotherapy strategy significantly enhances anticryptosporidial activity of an inhibitor of bifunctional thymidylate synthase-dihydrofolate reductase from *Cryptosporidium*, *Bioorg Med Chem Lett*, 25 (2015) 2065–2067. [PubMed: 25900220]
- [21]. Anderson AC, Two crystal structures of dihydrofolate reductase-thymidylate synthase from *Cryptosporidium hominis* reveal protein-ligand interactions including a structural basis for observed antifolate resistance, *Acta Crystallogr Sect F Struct Biol Cryst Commun*, 61 (2005) 258–262.
- [22]. Kumar VP, Cisneros JA, Frey KM, Castellanos-Gonzalez A, Wang Y, Gangjee A, White AC Jr., Jorgensen WL, Anderson KS, Structural studies provide clues for analog design of specific inhibitors of *Cryptosporidium hominis* thymidylate synthase-dihydrofolate reductase, *Bioorg Med Chem Lett*, 24 (2014) 4158–4161. [PubMed: 25127103]
- [23]. Czyzyk DJ, Valhondo M, Deiana L, Tirado-Rives J, Jorgensen WL, Anderson KS, Structure activity relationship towards design of cryptosporidium specific thymidylate synthase inhibitors, *Eur J Med Chem*, 183 (2019) 111673. [PubMed: 31536894]
- [24]. Landau MJ, Sharma H, Anderson KS, Selective peptide inhibitors of bifunctional thymidylate synthase-dihydrofolate reductase from *Toxoplasma gondii* provide insights into domain-domain communication and allosteric regulation, *Protein Sci*, 22 (2013) 1161–1173. [PubMed: 23813474]

- [25]. Martucci WE, Rodriguez JM, Vargo MA, Marr M, Hamilton AD, Anderson KS, Exploring novel strategies for AIDS protozoal pathogens: alpha-helix mimetics targeting a key allosteric protein-protein interaction in *C. hominis* TS-DHFR, *Medchemcomm*, 4 (2013).
- [26]. Ruiz V, Czyzyk DJ, Valhondo M, Jorgensen WL, Anderson KS, Novel allosteric covalent inhibitors of bifunctional *Cryptosporidium hominis* TS-DHFR from parasitic protozoa identified by virtual screening, *Bioorg Med Chem Lett*, 29 (2019) 1413–1418. [PubMed: 30929953]
- [27]. Anderson AC, O'Neil RH, DeLano WL, Stroud RM, The structural mechanism for half-the-sites reactivity in an enzyme, thymidylate synthase, involves a relay of changes between subunits, *Biochemistry*, 38 (1999) 13829–13836. [PubMed: 10529228]
- [28]. Johnson EF, Hinz W, Atreya CE, Maley F, Anderson KS, Mechanistic characterization of *Toxoplasma gondii* thymidylate synthase (TS-DHFR)-dihydrofolate reductase. Evidence for a TS intermediate and TS half-sites reactivity, *J Biol Chem*, 277 (2002) 43126–43136. [PubMed: 12192007]
- [29]. Perry KM, Pookanjanatavip M, Zhao J, Santi DV, Stroud RM, Reversible dissociation and unfolding of the dimeric protein thymidylate synthase, *Protein Sci*, 1 (1992) 796–800. [PubMed: 1304920]
- [30]. Berger SH, Berger FG, Lebioda L, Effects of ligand binding and conformational switching on intracellular stability of human thymidylate synthase, *Biochim Biophys Acta*, 1696 (2004) 15–22. [PubMed: 14726200]
- [31]. Almog R, Waddling CA, Maley F, Maley GF, Van Roey P, Crystal structure of a deletion mutant of human thymidylate synthase Delta (7–29) and its ternary complex with Tomudex and dUMP, *Protein Sci*, 10 (2001) 988–996. [PubMed: 11316879]
- [32]. Sayre PH, Finer-Moore JS, Fritz TA, Biermann D, Gates SB, MacKellar WC, Patel VF, Stroud RM, Multi-targeted antifolates aimed at avoiding drug resistance form covalent closed inhibitory complexes with human and *Escherichia coli* thymidylate synthases, *J Mol Biol*, 313 (2001) 813–829. [PubMed: 11697906]
- [33]. Phan J, Steadman DJ, Koli S, Ding WC, Minor W, Dunlap RB, Berger SH, Lebioda L, Structure of human thymidylate synthase suggests advantages of chemotherapy with noncompetitive inhibitors, *J Biol Chem*, 276 (2001) 14170–14177. [PubMed: 11278511]
- [34]. Chen D, Jansson A, Sim D, Larsson A, Nordlund P, Structural analyses of human thymidylate synthase reveal a site that may control conformational switching between active and inactive states, *J Biol Chem*, 292 (2017) 13449–13458. [PubMed: 28634233]
- [35]. Cardinale D, Guaitoli G, Tondi D, Luciani R, Henrich S, Salo-Ahen OM, Ferrari S, Marverti G, Guerrieri D, Ligabue A, Frassinetti C, Pozzi C, Mangani S, Fessas D, Guerrini R, Ponterini G, Wade RC, Costi MP, Protein-protein interface-binding peptides inhibit the cancer therapy target human thymidylate synthase, *Proc Natl Acad Sci U S A*, 108 (2011) E542–549. [PubMed: 21795601]
- [36]. Tochowicz A, Santucci M, Saxena P, Guaitoli G, Trande M, Finer-Moore J, Stroud RM, Costi MP, Alanine mutants of the interface residues of human thymidylate synthase decode key features of the binding mode of allosteric anticancer peptides, *J Med Chem*, 58 (2015) 1012–1018. [PubMed: 25427005]
- [37]. Lovelace LL, Minor W, Lebioda L, Structure of human thymidylate synthase under low-salt conditions, *Acta Crystallogr D Biol Crystallogr*, 61 (2005) 622–627. [PubMed: 15858273]
- [38]. Sharma H, Landau MJ, Sullivan TJ, Kumar VP, Dahlgren MK, Jorgensen WL, Anderson KS, Virtual screening reveals allosteric inhibitors of the *Toxoplasma gondii* thymidylate synthase-dihydrofolate reductase, *Bioorg Med Chem Lett*, 24 (2014) 1232–1235. [PubMed: 24440298]
- [39]. Atreya CE, Anderson KS, Kinetic characterization of bifunctional thymidylate synthase-dihydrofolate reductase (TS-DHFR) from *Cryptosporidium hominis*: a paradigm shift for its activity and channeling behavior, *J Biol Chem*, 279 (2004) 18314–18322. [PubMed: 14966126]
- [40]. Prasanna V, Bhattacharjya S, Balaram P, Synthetic interface peptides as inactivators of multimeric enzymes: inhibitory and conformational properties of three fragments from *Lactobacillus casei* thymidylate synthase, *Biochemistry*, 37 (1998) 6883–6893. [PubMed: 9578575]

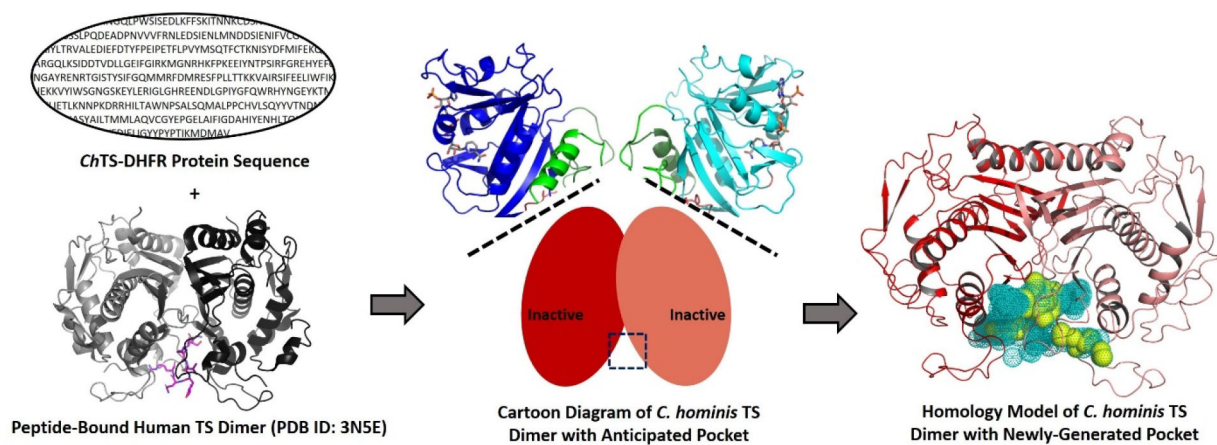


Figure 1. Homology model of *C. hominis* TS created using the amino acid sequence of *ChTS* and the peptide-bound human TS structure. The newly-generated binding pocket is shown as dots (teal) and spheres (yellow). The hydrophobic parts of the pocket, including the buried hydrophobic cavity, are highlighted as spheres in yellow.

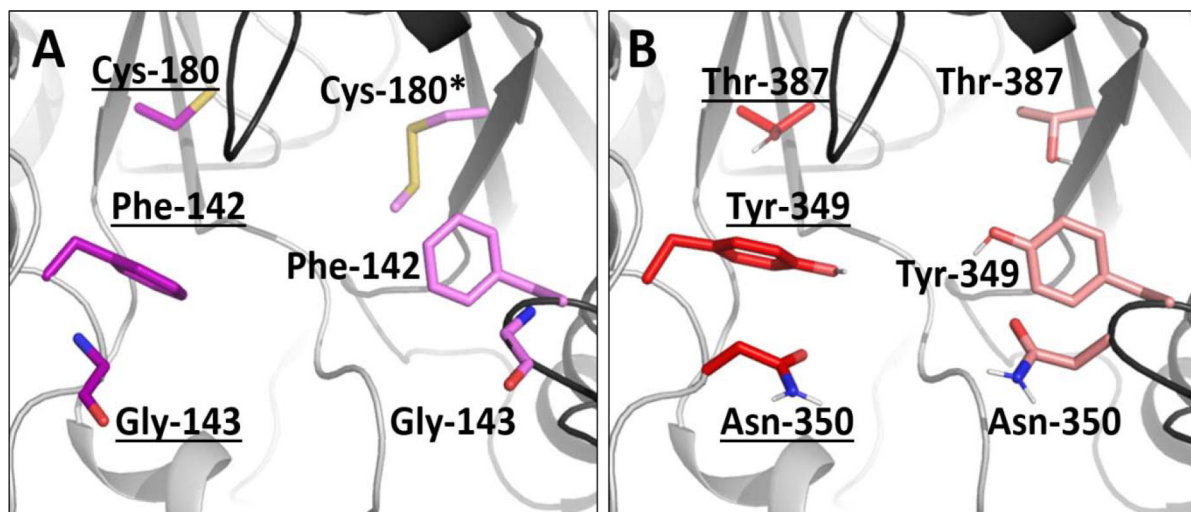


Figure 2. Differences between human TS (A, PDB ID: 3N5E) and our *ChTS* homology model (B) at the TS/TS interface. Residues Phe-142, Gly-143, and Cys-180 in human TS (A, purple and hot pink) correspond to residues Tyr-349, Asn-350, and Thr-387, respectively, in the *C. hominis* enzyme (B, red and light pink). We took advantage of these differences in our virtual screen to search for *Ch*-specific inhibitors. Note that Cys-180* was mutated to S-methylthiocysteine in the human structure to help with crystallization.

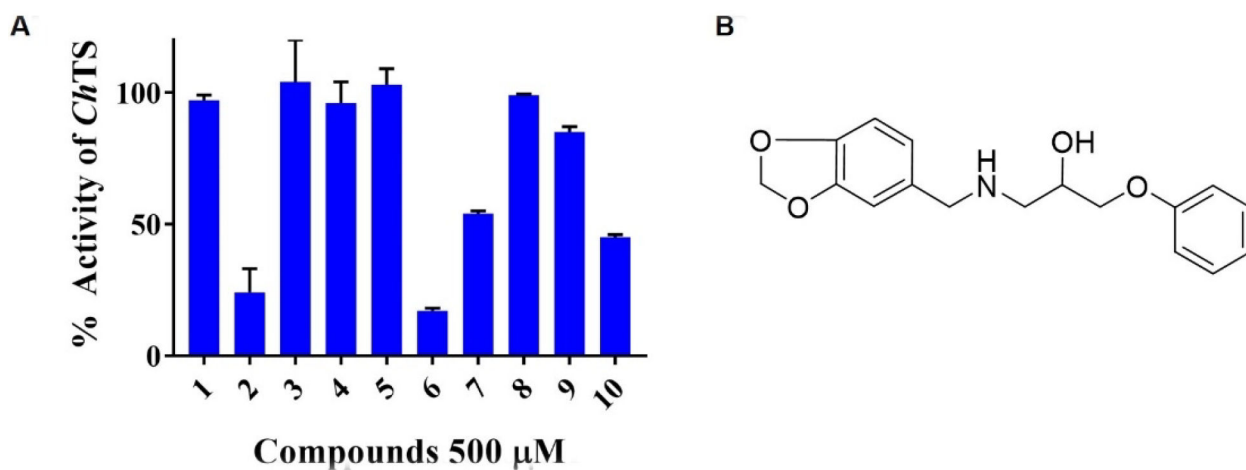


Figure 3.

(A) *ChTS* Inhibition for the ten compounds selected from our virtual screen. The y-axis denotes *ChTS* percent activity in the presence of 500 μM compound. (B) Two-dimensional structure depicting the common chemotype of three methylenedioxyphenyl-aminophenoxypropanol compounds, **2**, **6**, and **10**, identified by our virtual screen and determined to be inhibitors of *ChTS* activity.

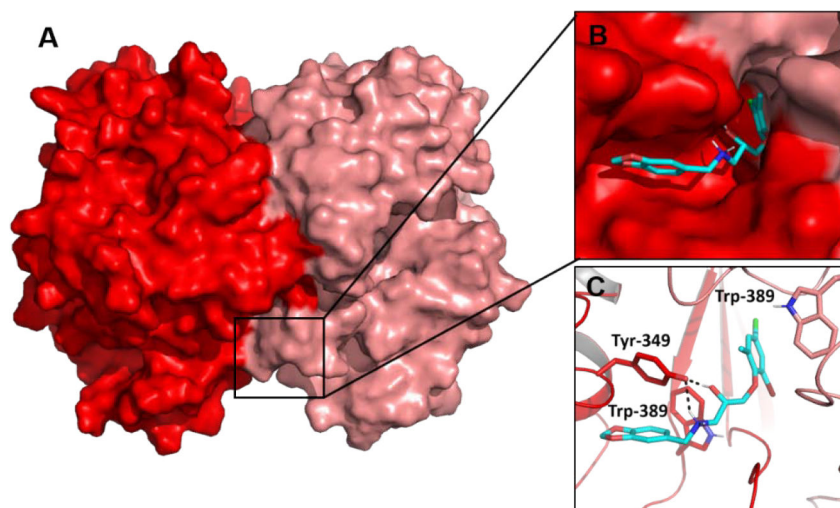
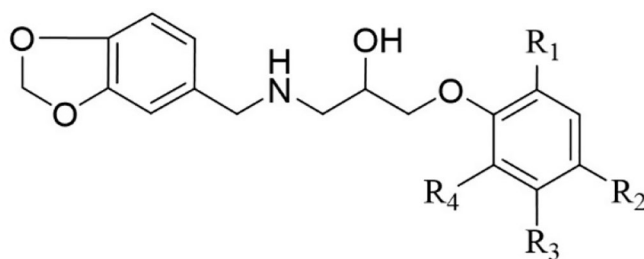


Figure 4. Docked model of Cpd **6** (HTS 00950, cyan) bound to the *ChTS*/TS interface. Cpd **6** was identified by our virtual screen and determined to be our best inhibitor of *ChTS* activity.



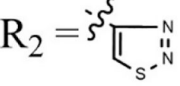
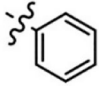
Cpd 2	Cpd 6	Cpd 14	Cpd 18
$R_1 = H$	$R_1 = CH_3$	$R_1 = H$	$R_1 = H$
$R_2 =$ 	$R_2 = Cl$	$R_2 =$ 	$R_2 = Cl$
$R_3 = H$	$R_3 = H$	$R_3 = H$	$R_3 = Cl$
$R_4 = H$	$R_4 = Br$	$R_4 = H$	$R_4 = H$

Figure 5. Similarities and differences between the four methylenedioxyphenyl-aminophenoxypropanol derivatives with greater than 75% inhibition of *ChTS* activity at 500 μ M.

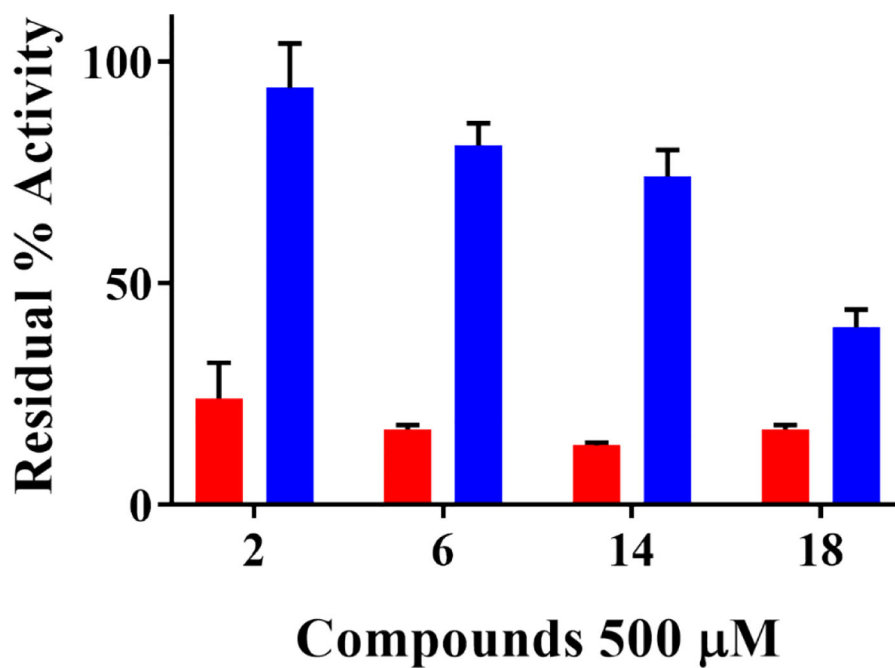


Figure 6. Selective inhibition of *ChTS* activity over *ChDHFR* activity by compounds **2**, **6**, **14**, and **18**. Residual *ChTS* percent activity upon inhibition is shown in red. Residual *ChDHFR* percent activity is shown in blue.

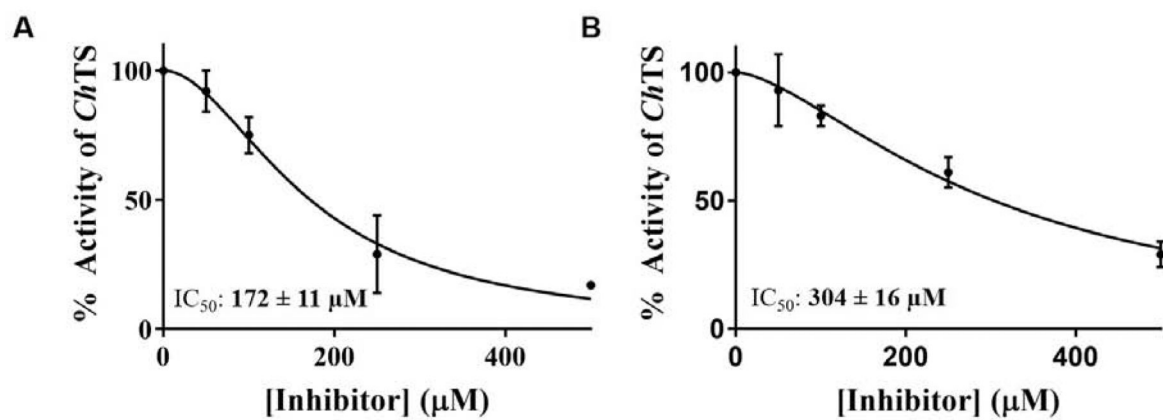


Figure 7. Preferential binding of compound **6** to the inactive conformation of *ChTS*. *ChTS* activity was measured at varying concentrations of **6**. The plot in (A) denotes dose-dependent inhibition when **6** was mixed with *ChTS* in the absence of dUMP (inactive conformation). The plot in (B) denotes dose-dependent inhibition when **6** was mixed with *ChTS* in the presence of dUMP (active conformation).

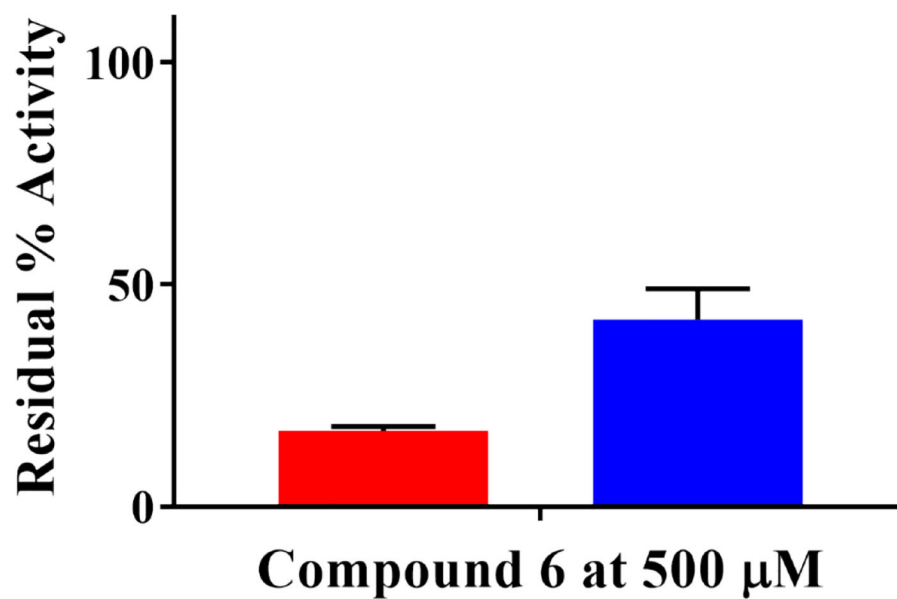


Figure 8. Selective inhibition of *ChTS* activity over *hTS* activity by compound **6**. Residual *ChTS* percent activity upon inhibition is shown in red; Residual *hTS* percent activity is shown in blue.

Table 1

Experimental evaluation of top 10 virtual screen compounds ranked by GLIDE XP

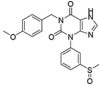
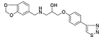
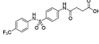
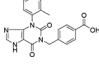
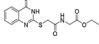
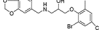
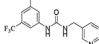
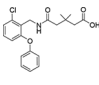
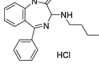
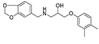
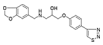
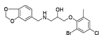
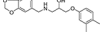
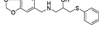
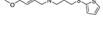


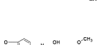
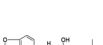
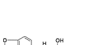


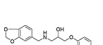

Compound No.	Maybridge Identification Code	GLIDE XP Score	Chemical Structure	% Inhibition of ChTS Activity at 500 μ M
1	KM 10219	-10.211		< 5
2	HTS 03850	-10.186		76 \pm 9
3	GK 02743	-10.170		No inhibition
4	KM 10022	-10.104		< 5
5	JFD 02033	-10.000		No inhibition
6	HTS 00950	-9.999		83 \pm 1
7	CD 11057	-9.977		46.0 \pm 0.8
8	HTS 02399	-9.863		No inhibition
9	BTB 15245	-9.845		15 \pm 2
10	HTS 00967	-9.792		55 \pm 1

Table 2

SAR of methylenedioxyphenyl-aminophenoxypropanol derivative compounds

Compound No.	Vendor and Identification Code	Chemical Structure	% Inhibition of ChTS Activity at 500 μ M
2	Maybridge HTS 03850		76 \pm 9
6	Maybridge HTS 00950		83 \pm 1
10	Maybridge HTS 00967		55 \pm 1
11	Maybridge HTS 00807		34 \pm 4
12	Maybridge HTS 00959		43 \pm 11
13	Maybridge HTS 02908		< 5
14	Enamine Z31367869		87 \pm 1
15	Enamine Z235247810		< 5
16	Enamine Z55679604		20 \pm 6
17	Enamine Z57990126		48 \pm 9
18	Chemspace PB31445275		83 \pm 1
19	Chemspace PB31445326		55 \pm 6
20	Chemspace PB31445328		26 \pm 4
21	Chemspace PB31445377		7 \pm 1